

Visibility of current and shot noise in electrical Mach-Zehnder and Hanbury Brown Twiss interferometers

V.S.-W. Chung^{1,2}, P. Samuelsson³, and M. Büttiker¹

¹*Département de Physique Théorique, Université de Genève, Genève 4, CH-1211 Switzerland*

²*Department of Electronics, National Chiao-Tung University, Hsinchu 30010, Taiwan*

³*Division of Solid State Theory, Lund University, Sölvegatan 14 A, S-223 62 Lund, Sweden*

(Dated: September 3, 2018)

We investigate the visibility of the current and shot-noise correlations of electrical analogs of the optical Mach-Zehnder interferometer and the Hanbury Brown Twiss interferometer. The electrical analogs are discussed in conductors subject to high magnetic fields where electron motion is along edge states. The transport quantities are modulated with the help of an Aharonov-Bohm flux. We discuss the conductance (current) visibility and shot noise visibility as a function of temperature and applied voltage. Dephasing is introduced with the help of fictitious voltage probes. Comparison of these two interferometers is of interest since the Mach-Zehnder interferometer is an amplitude (single-particle) interferometer whereas the Hanbury Brown Twiss interferometer is an intensity (two-particle) interferometer. A direct comparison is only possible for the shot noise of the two interferometers. We find that the visibility of shot noise correlations of the Hanbury Brown Twiss interferometer as function of temperature, voltage or dephasing, is qualitatively similar to the visibility of the first harmonic of the shot noise correlation of the Mach-Zehnder interferometer. In contrast, the second harmonic of the shot noise visibility of the Mach-Zehnder interferometer decreases much more rapidly with increasing temperature, voltage or dephasing rate.

PACS numbers: 72.10.-d, 72.70.+m, 73.43.-f

I. INTRODUCTION

With the advent of mesoscopic physics, it has become possible to experimentally investigate quantum phase coherent properties of electrons in solid state conductors in a controlled way. In particular, in ballistic mesoscopic samples at low temperatures, electrons can propagate up to several microns without losing phase information. This opens up the possibility to investigate electrical analogs of various optical phenomena and experiments. An investigation of such analogs is of fundamental interest. On the one hand, it allows one to establish similarities between the properties of photons and conduction electrons, a consequence of the wave nature of the quantum particles. On the other hand, it also allows one to investigate the differences between the two types of particles arising from the different quantum statistical properties of fermions and bosons. For many-particle properties, such as light intensity correlations or correspondingly electrical current correlations, noise, the quantum statistical properties are important.^{1,2} Both the wave-nature of the particles as well as their quantum statistics are displayed in a clearcut fashion in interferometer structures. In this work we are concerned with the electrical analogs of two well known optical interferometers, the single-particle Mach-Zehnder (MZ) interferometer and the two-particle Hanbury Brown Twiss (HBT) interferometer.

The MZ-interferometer is a subject of most textbooks in optics.³ In the framework of quantum optics, considering individual photons rather than classical beams of light, the interference arises due to the superposition of the amplitudes for two different possible paths of a sin-

gle photon. This leads to an interference term in the light intensity. The MZ-interferometer is thus a prime example of a single particle interferometer.⁴ Various electronic interferometers with ballistic transport of the electrons have been investigated experimentally over the last decades, as e.g. Aharonov-Bohm (AB) rings⁵ and double-slit interferometers.⁶ Detailed investigations of dephasing in ballistic interferometers was carried out in Refs. [7,8]. Only very recently was the first electronic MZ-interferometer realized by Ji et al.⁹ in a mesoscopic conductor in the quantum Hall regime. A high visibility of the conductance oscillations was observed, however the visibility was not perfect. This led the authors to investigate in detail various sources for dephasing. As a part of this investigation, also shot noise was measured. Still, some aspects of the experiment are not yet fully understood. Theoretically, Seelig and one of the authors¹⁰ investigated the effect of dephasing due to Nyquist noise on the conductance in a MZ-interferometer. The effect of dephasing on the closely related four-terminal resistance in ballistic interferometers¹¹ was investigated as well. Dephasing in ballistic strongly interacting systems is discussed by Le Hur.^{12,13} Following the experimental work of Ji et al.,⁹ Marquardt and Bruder investigated the effect of dephasing on the shot-noise in MZ-interferometers, considering dephasing models based on both classical^{14,15} as well as quantum fluctuating fields.¹⁶ Very recently, Förster, Pilgram and one of the authors¹⁷ extended the dephasing model of Refs. [10,14] to the full statistical distribution of the transmitted charge.

The HBT-interferometer^{18,19,20} was originally invented for stellar astronomy, to measure the angular diameter of stars. It is an intensity, or two-particle,⁴ interferome-

ter. The interference arises from the superposition of the amplitudes for two different two-particle processes. Importantly, there is no single particle interference in the HBT-interferometer. Consequently, in contrast to the MZ-interferometer there is no interference in the light intensity, the interference instead appears in the intensity-intensity correlations. Moreover, the intensity-intensity correlation also display the effect of quantum statistics. Photons originating from thermal sources tend to bunch, giving rise to positive intensity cross correlations. For the electronic analog of the HBT-interferometer, it was the corresponding anti-bunching of electrons that originally attracted interest. It was predicted¹ that the electrical current cross correlations in mesoscopic conductors would be manifestly negative, i.e. display anti-bunching, as a consequence of the fermionic statistics of the electrons. Negative current cross correlations were subsequently observed in two independent experiments.^{21,22} Recently, anti-bunching for field emitted electrons in vacuum was also demonstrated.²³ The two-particle interference in the HBT-experiment has received much less attention. We emphasize that while the bunching of the photons was necessary for obtaining a finite, positive cross correlation signal, it was the two-particle effect that was of main importance to HBT since the angular diameter of the star was determined from the two-particle interference pattern. In electrical conductors, two-particle effects in AB-interferometers were investigated theoretically in Refs. [24,25,26]. Only very recently two of the authors and Sukhorukov²⁷ proposed a direct electronic analog of the optical HBT-interferometer which permits to demonstrate two-particle interference in an unambiguous way.

In this work we investigate and compare in detail the current and zero-frequency noise in electronic MZ and HBT interferometers. We consider interferometers implemented in mesoscopic conductors in the integer Quantum Hall regime, where the transport takes place along single edge states and Quantum Point Contacts (QPC's) serve as controllable beam splitters. The effect of finite temperature, applied bias and asymmetry, i.e. unequal length of the interferometer arms, is investigated. The strength of the interference contribution is quantified via the visibility of the phase oscillations. The dependence of the visibility on the beam splitter transparencies as well as on the temperature, voltage and asymmetry is discussed in detail. Of interest is the comparison of visibility of the shot-noise correlation of the MZ-interferometer and the HBT-intensity interferometer. Shot noise correlations in the MZ-interferometer exhibit two contributions, one with the fundamental period of h/e and a second harmonic with period $h/2e$. The shot noise correlations in the HBT-interferometer, even though they are due to two particle processes, are periodic with period h/e . Thus the Aharonov-Bohm period can not be used to identify the two particle processes which give rise to the HBT effect. It is therefore interesting to ask whether the HBT two-particle processes

have any other signature, for instance in the temperature or voltage dependence of the visibility of the shot-noise correlation. We find that this is not the case. To the contrary, we find that the the shot noise correlations in the HBT intensity interferometer behave qualitatively similar to the h/e shot noise correlation in the MZ-interferometer. In contrast the $h/2e$ contribution in the shot noise of the MZ-interferometer decreases more rapidly with increasing temperature, voltage or dephasing rate than the h/e oscillation in the MZ- or HBT-interferometer.

We investigate dephasing of the electrons propagating along the edge states by connecting one of the interferometer arms to a fictitious, dephasing voltage probe. In all cases, the current and noise of the MZ-interferometer as well as the noise in the HBT-interferometer, the effect of the voltage probe is equivalent to the effect of a slowly fluctuating phase.

II. MODEL AND THEORY

A. Optical analogs in the Quantum Hall regime

In the paper we consider implementations of the MZ and HBT interferometers in mesoscopic conductors in strong magnetic fields, in the integer Quantum Hall regime.²⁸ The typical system is a two-dimensional electron gas in a semiconductor heterostructure, with the lateral confinement of the electron gas controllable via electrostatic gating. The transport between reservoirs²⁹ connected to the conductor takes place along edge states.³⁰ The edge states, quantum analogs of classical skipping orbits, are chiral, the transport along an edge state is unidirectional. Scattering between edge states is suppressed everywhere in the conductor except at electrostatically controllable constrictions, QPC's.^{31,32} For a magnetic field that does not break the spin degeneracy of the edge states, each edge state supplies two conduction modes, one per spin.

These properties make conductors in the integer quantum Hall regime ideal for realizing analogs of optical experiments. First, the edge states correspond to single mode waveguides for the light. The unidirectional motion along the edge states allows for "beams" of electrons to be realized. Second, the QPC's work as electronic beam splitters with controllable transparency. Moreover, due to chirality the beamsplitters are reflectionless, a property essential for the MZ and HBT interferometers but difficult to achieve for beam splitters in conductors in weak (or zero) magnetic fields.^{22,33} These properties of conductors in the quantum Hall regime have been demonstrated experimentally in a number of works, see e.g. [9,21,34].

Theoretically, several works have been concerned with the conductance and noise properties of beam splitters and interferometers in Quantum Hall systems, for a recent reviews see e.g. Refs. [2,35]. Recently, it was pro-

posed to use these appealing properties of edge states in the context of orbital³⁶ quasi-particle entanglement in static^{27,37,38} and dynamic^{39,40} systems as well as for quantum state transfer.⁴¹

It is interesting to note that the edge state description also hold for conductors at even higher magnetic fields, in the fractional Quantum Hall regime. As examples, the fractional charge has been determined in shot-noise experiments^{42,43} and the quantum statistical properties of the fractionally charged quasi-particles have been investigated theoretically in beam-splitter⁴⁴ and HBT⁴⁵ geometries. Various interferometer structures have also been considered.^{46,47,48} Very recently, a MZ-interferometer in the fractional Quantum Hall regime was proposed.⁴⁹ In this work we however consider only the integer Quantum Hall effect, where the quasi-particles are noninteracting and the electrical analogs to optical experiments can be directly realized.

B. Scattering approach to current and noise

This discussion leads us to consider single mode, multi-terminal conductors with noninteracting electrons. The principle aim of this work is a comparison of the MZ and HBT-interferometers. In reality in both interferometers interactions (screening) play a role both for the voltage and temperature dependence. A non-interacting scattering approach is not gauge invariant but requires a treatment of screening.⁵⁰ However, these effects are expected to be similar in the two interferometers and will not affect the main conclusions of this work. Therefore, below we treat non-interacting quasi-particle interferometers. The conductors are connected to several electronic reservoirs, biased at a voltage eV or grounded. The current⁵¹ and the noise^{1,52} are calculated within the scattering approach for multi-terminal conductors. We first introduce the creation and annihilation operators for incoming, $\hat{a}_\alpha^\dagger(E)$ and $\hat{a}_\alpha(E)$, and outgoing, $\hat{b}_\alpha^\dagger(E)$ and $\hat{b}_\alpha(E)$, particles, at energy E in terminal α . For simplicity we suppress spin notation. Considering a conductor with N terminals, the in- and out-going annihilation operators are related via the $N \times N$ scattering matrix, as

$$\hat{b}_\alpha(E) = \sum_{\beta=1}^N s_{\alpha\beta}(E) \hat{a}_\beta(E) \quad (1)$$

where $s_{\alpha\beta}(E)$ is the amplitude to scatter from terminal β to terminal α . The current operator in the lead α has the form⁵¹

$$\begin{aligned} \hat{I}_\alpha(t) &= \frac{e}{h} \sum_{\beta\gamma} \int dE dE' \exp(i[E - E']t/\hbar) \\ &\times A_{\beta\gamma}^\alpha(E, E') \hat{a}_\beta^\dagger(E) \hat{a}_\gamma(E'), \end{aligned} \quad (2)$$

with the notation

$$A_{\beta\gamma}^\alpha(E, E') = \delta_{\alpha\beta} \delta_{\alpha\gamma} - s_{\alpha\beta}^*(E) s_{\alpha\gamma}(E'). \quad (3)$$

The average current is given by⁵¹

$$\langle I_\alpha \rangle = \int dE j_\alpha(E), \quad (4)$$

where the spectral current density is

$$j_\alpha(E) = \frac{1}{e} \sum_{\beta} G_{\alpha\beta}(E) f_\beta(E). \quad (5)$$

Here $f_\beta(E) = 1/(1 + \exp[(E - eV_\beta)/k_B T])$ is the Fermi Dirac distribution of terminal β , with V_β the corresponding applied voltage. The spectral conductance $G_{\alpha\beta}(E)$ is given by

$$G_{\alpha\beta}(E) = \frac{e^2}{h} A_{\beta\beta}^\alpha(E, E). \quad (6)$$

The zero frequency correlator between current fluctuations in terminals α and β is defined as

$$S_{\alpha\beta} = \int dt \langle \Delta \hat{I}_\alpha(0) \Delta \hat{I}_\beta(t) + \Delta \hat{I}_\beta(t) \Delta \hat{I}_\alpha(0) \rangle, \quad (7)$$

where $\Delta \hat{I}_\alpha(t) = \hat{I}_\alpha(t) - \langle \hat{I}_\alpha(t) \rangle$. The current correlator is given by^{1,52}

$$S_{\alpha\beta} = \int dE S_{\alpha\beta}(E) \quad (8)$$

where

$$\begin{aligned} S_{\alpha\beta}(E) &= \frac{2e^2}{h} \sum_{\gamma\delta} A_{\gamma\delta}^\alpha(E, E) A_{\delta\gamma}^\beta(E, E) \\ &\times f_\gamma(E) [1 - f_\delta(E)] \end{aligned} \quad (9)$$

is the spectral current correlator.

C. Dephasing voltage probe model

There are several physical mechanisms that might lead to dephasing of the electrons propagating along the edge states (see e.g. the discussion in Ref. [9]). In this work we are not interested in any particular mechanism for dephasing but consider instead a phenomenological model, a dephasing voltage probe. The idea of using a voltage probe to induce dephasing was introduced in Refs. [53,54]. A voltage probe connected to a mesoscopic sample was considered, leading to a suppression of coherent transport due to inelastic scattering. The probe model, originally considered for the average current, was extended to treat the effect of inelastic scattering on shot noise by Büttiker and Beenakker⁵⁵ by considering a conservation of current fluctuations at the probe as well. Later De Jong and Beenakker⁵⁶ extended the voltage probe concept and introduced a (fictitious) voltage probe which breaks phase but does not dissipate energy. Scattering in the voltage probe is (quasi-)elastic.

This is achieved with the help of a distribution function in the voltage probe which conserves not only total current like a real voltage probe, but conserves current in every small energy interval. Such a probe provides a model of pure dephasing. The different probe models have been used as qualitative models in a number of works, see Refs. [2,57] for a review. For an application to quantum Hall systems, see Ref. [58].

In this work we consider the dephasing voltage probe model, which conserves the current at each energy. The model is based on the assumption that the current is conserved on a time scale τ_C , much shorter than the time of the measurement but much longer than the time between injection of individual electrons, here of the order of \hbar/eV . One could however consider a more general voltage probe model that takes into account a more complicated dynamics of the probe. A detailed discussion of such a general model in the light of recent work^{14,15,59,60} is however deferred to a later work. Here we only note that below we find that the voltage probe in both the MZ and HBT-interferometers only gives rise to a suppression of the phase dependent terms in conductance and noise, just as one would naively expect to be the effect of pure dephasing.

The condition of zero current into the fictitious probe γ at each energy is fulfilled by considering a time dependent distribution function of the probe

$$f_\gamma(E, t) = \bar{f}_\gamma(E) + \delta f_\gamma(E, t), \quad (10)$$

where $\delta f_\gamma(E, t)$ fluctuates to conserve current on the timescale τ_C . As a consequence, the spectral current density at each energy in lead α fluctuates in time as

$$j_\alpha(E, t) = j_\alpha(E) + \Delta j_\alpha(E, t), \quad (11)$$

where the fluctuations $\Delta j_\alpha(E, t) = \delta j_\alpha(E, t) + (1/e)G_{\alpha\gamma}(E)\delta f_\gamma(E, t)$ consist of two parts, the intrinsic fluctuations $\delta j_\alpha(E, t)$ and the additional fluctuations due to $\delta f_\gamma(E, t)$. The requirement of zero average current into the probe, $j_\gamma(E) = 0$, leads to the averaged distribution function at the probe reservoir γ

$$\bar{f}_\gamma(E) = - \sum_{\alpha \neq \gamma} \frac{G_{\gamma\alpha}(E)}{G_{\gamma\gamma}(E)} f_\alpha(E). \quad (12)$$

The average spectral current density $j_\alpha^{dp}(E)$ is then found from Eq. (5).

The fluctuating part of the distribution function, $\delta f_\gamma(E, t)$, is obtained from the requirement of zero current fluctuations into the probe, $\Delta j_\gamma(E, t) = \delta j_\gamma(E, t) + (1/e)G_{\gamma\gamma}(E)\delta f_\gamma(E, t) = 0$. The total current density fluctuation is then given by

$$\Delta j_\alpha(E, t) = \delta j_\alpha(E, t) - \frac{G_{\alpha\gamma}(E)}{G_{\gamma\gamma}(E)} \delta j_\gamma(E, t). \quad (13)$$

As a result, in the presence of dephasing the total spectral

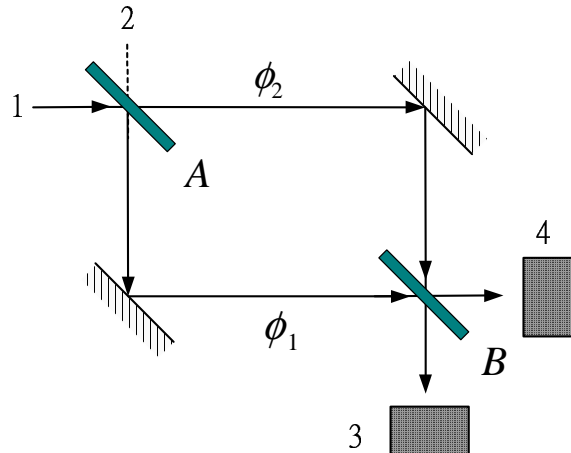


FIG. 1: An optical Mach-Zehnder interferometer. A beam of light incident from 1 is split in two partial beams at the semitransparent beam splitter A . The two partial beams acquire geometrical phases ϕ_1 and ϕ_2 respectively and are rejoined at the second beam splitter B . The light intensity is measured in detectors 3 and 4

current correlation $S_{\alpha\beta}^{dp}(E)$ is

$$S_{\alpha\beta}^{dp}(E) = S_{\alpha\beta}(E) - \frac{G_{\alpha\gamma}(E)}{G_{\gamma\gamma}(E)} S_{\beta\gamma}(E) - \frac{G_{\beta\gamma}(E)}{G_{\gamma\gamma}(E)} S_{\alpha\gamma}(E) + \frac{G_{\alpha\gamma}(E)G_{\beta\gamma}(E)}{G_{\gamma\gamma}^2(E)} S_{\gamma\gamma}(E), \quad (14)$$

where $S_{\alpha\beta}(E)$ is the correlation function between the intrinsic current fluctuations, δj_α and δj_β , of contact α and β , given by Eq. (9), and $G_{\alpha\beta}(E)$ is the conductance, given by Eq. (6).

III. MACH-ZEHNDER INTERFEROMETERS

A schematic of the MZ-interferometer is shown in Fig. 1. An incident beam of light from source 1 is divided in two parts at the semitransparent beam splitter A . The two partial beams are reflected at mirrors and later joined at the second beam splitter B . Beams of light going out from B are detected in 3 and 4. The amplitude of the light in an outgoing beam is the sum of the amplitudes for the two partial beams, $A = A_1 \exp(i\phi_1) + A_2 \exp(i\phi_2)$. This gives an intensity $|A|^2 = |A_1|^2 + |A_2|^2 + 2\text{Re}\{A_1 A_2^* \exp(i[\phi_1 - \phi_2])\}$. The interference term $2\text{Re}\{A_1 A_2^* \exp(i[\phi_1 - \phi_2])\}$ thus contains the difference between the geometrical phases, $\phi_1 - \phi_2$. Importantly, the four terminal geometry together with the reflectionless beam splitters lead to that the incident beam traverses the interferometer only once. This is a defining property of the MZ-interferometer.

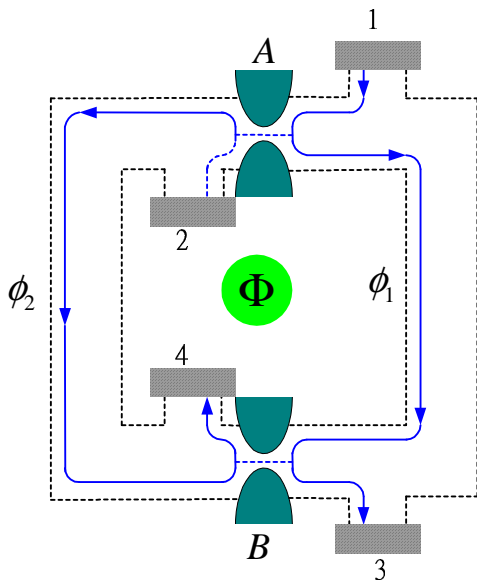


FIG. 2: The electronic analog of the MZ-interferometer, implemented by Ji et al.⁹ in a conductor in the Quantum Hall regime. The electronic reservoir 1 is biased at eV and reservoirs 2 to 4 are kept at ground. The edge states (solid lines) have a direction of transport indicated by arrows. The QPC's A and B play the role of the beam splitters in Fig. 1. Geometrical phases ϕ_1 and ϕ_2 and the AB-flux Φ are shown.

We then turn to the electric analog of the MZ-interferometer, shown in Fig. 2. As pointed out above, several results for the current and noise are available in the literature.^{10,11,14,15,16,17} Here we analyze the most general situation possible, with finite voltage, temperature and interferometer arm asymmetry as well as different beam splitters A and B with arbitrary transparency. When we consider limiting cases for e.g. small temperature, bias or asymmetry, known results are recovered. This detailed analysis of the MZ-interferometer is of importance when comparing to the HBT-interferometer below.

We first discuss a fully coherent interferometer, the effect of dephasing is investigated below. An electric potential eV is applied at terminal 1, all other terminals are kept at zero potential. The injected electrons propagate along single edge states. Scattering between the edge states can take place only at the two QPC's, acting as beam splitters with controllable transparency. The beam splitters $j = A, B$ are characterized by the scattering matrices

$$\begin{pmatrix} i\sqrt{R_j} & \sqrt{T_j} \\ \sqrt{T_j} & i\sqrt{R_j} \end{pmatrix}, \quad (15)$$

where T_j and $R_j = 1 - T_j$ are the transmission and reflection probabilities, respectively. We note that any additional phases of the beam splitters just give rise to a

constant phase shift of the oscillations in the interference terms and are therefore not considered.

Propagating along the edge states, the electrons pick up geometrical phases ϕ_1 and ϕ_2 as well as phases ψ_1 and ψ_2 due to the AB-flux Φ through the center of the interferometer. For example, the amplitude for scattering from terminal 1 to 4 is given by

$$s_{41} = i\sqrt{T_B R_A} e^{i(\phi_1 + \psi_1)} + i\sqrt{T_A R_B} e^{i(\phi_2 - \psi_2)} \quad (16)$$

For the geometrical phases, to be specific we consider the case when the potential landscape $eU(x, y)$ of the conductor in Fig. 2 is varying smoothly on the scale of the magnetic length $l_B = (\hbar/e|B|)^{1/2}$, with $B\hat{z}$ the applied magnetic field perpendicular to the plane in Fig. 2 (the effect of self-consistency of the potential⁶¹ is neglected). This allows for a semiclassical treatment.⁶² In a high magnetic field the edge states at Fermi energy E_F follow equipotential lines determined by $eU(x, y) = E_F - \hbar\omega_c(n + 1/2)$ where $\omega_c = eB/m$ is the cyclotron frequency and m the effective electron mass. We are concerned here with the case where there is only one edge state and thus $n = 0$. Suppose the x -axis is a line intersecting quantum point contacts A and B in Fig. 2. Excluding self-intersections we can express the edge state in terms of functions $y_1(x)$ and $y_2(x)$ for the left and right path of the interferometer. Working in the symmetric gauge, the geometric phases can be written⁶² $\phi_i = -l_B^{-2} \int_{x_A}^{x_B} dx y_i(x)$, where x_A and x_B are the locations of the QPC's. Importantly, $\phi_1 - \phi_2$ corresponds to the total area A enclosed by these two paths divided by the magnetic length squared, or $\phi_1 - \phi_2 = 2\pi BA/\Phi_0$ where BA is the total flux through the enclosed area and $\Phi_0 = h/e$ the elementary flux quantum. Note that the Aharonov-Bohm flux Φ adds an additional phase ψ_1 and ψ_2 , with $\psi_1 + \psi_2 = 2\pi\Phi/\Phi_0$, to each of the paths.

For the discussion of the temperature and voltage dependence of the current and the noise, we also need to know the energy dependence of the phases. First, instead of parameterizing the edge state through x we introduce the parameter s which measures directly the path length, i.e. $x(s), y(s)$. In addition at s we introduce local coordinates s_{\parallel} along and s_{\perp} perpendicular to the equipotential line. In these coordinates, an edge state that follows the equipotential line at a small energy E away from E_F acquires the additional phase $\Delta\phi = -l_B^{-2} \int ds \Delta s_{\perp}$ with $e(dU/ds_{\perp})\Delta s_{\perp} = E$. The potential gradient dU/ds_{\perp} determines the local electric field $F(s) = -dU/ds_{\perp}$ at s . But $eF(s)l_B = \hbar v_D(s)$ where $v_D(s) = F(s)/B$ is the drift velocity of the guiding center of the cyclotron orbit at point s of the edge state. Thus a small increase in energy leads to a phase increment given by $\Delta\phi_i = \int ds [1/\hbar v_D(s)] E$. A rough estimate using a drift velocity which is constant along the edge gives $\Delta\phi_i \approx (L_i/\hbar v_D) E$ with L_i the length of the edge state i . For the phase-difference of the two interfering paths we have

$$\phi_1(E) - \phi_2(E) = \Delta\phi(E_F) + E/E_c \quad (17)$$

with $\Delta\phi(E_F) = \phi_1(E_F) - \phi_2(E_F)$ the equilibrium phase difference. Formally, higher order terms in energy can be neglected for characteristic energies $k_B T$ and eV much smaller than $(dU/ds_\perp)^2/[d^2U/ds_\perp^2]$. The asymmetry of the two edges thus gives rise to an energy scale $E_c = \{\int ds[1/\hbar v_D(s_1)] - \int ds[1/\hbar v_D(s_2)]\}^{-1}$ which is due to the mismatch of the edge state path lengths, i.e. $E_c \approx \hbar v_D/(\Delta L)$ with $\Delta L = L_1 - L_2$. In principle, for a completely symmetric interferometer one has $E_c \rightarrow \infty$.

Given the scattering amplitudes $s_{\alpha\beta}$, the spectral current density is found from Eqs. (3), (5) and (6). For e.g. terminal 4, one gets

$$j_4(E) = (\epsilon/h) [f(E) - f_0(E)] [\mathcal{T}_A R_B + \mathcal{T}_B R_A + 2\sqrt{\mathcal{T}_A \mathcal{T}_B R_A R_B} \cos(E/E_c + \Theta)], \quad (18)$$

where we introduce the total, energy independent phase $\Theta = \Delta\phi(E_F) + 2\pi\Phi/\Phi_0$. Here $f_0(E)$ is the distribution functions of the grounded terminals 2,3 and 4 and $f(E) = f_0(E - eV)$ the distribution function of terminal 1. The current is then given from Eq. (4), as

$$I_4 = \frac{e}{h} \left[(\mathcal{T}_A R_B + \mathcal{T}_B R_A) eV + \sqrt{\mathcal{T}_A \mathcal{T}_B R_A R_B} \times 4\pi k_B T \text{csch}\left(\frac{k_B T \pi}{E_c}\right) \sin\left(\frac{eV}{2E_c}\right) \cos\left(\frac{eV}{2E_c} + \Theta\right) \right]. \quad (19)$$

Current conservation gives $I_3 = (e^2/h)V - I_4$. The current consists of two physically distinct parts. The first term in Eq. (19) is the phase independent, incoherent part, the current in the absence of interference, while the second, phase dependent term is the interference contribution. We note that a bias eV of the order of the asymmetry energy E_c leads to the phase shifts of the oscillation. The strength of the interference can conveniently be quantified via the visibility as

$$\nu_I = \frac{I_{\max} - I_{\min}}{I_{\max} + I_{\min}} = \frac{\text{amp}[I]}{\langle I \rangle}, \quad (20)$$

which gives for the current in the MZ-interferometer

$$\nu_{I,MZ} = \frac{\sqrt{\mathcal{T}_A \mathcal{T}_B R_A R_B}}{\mathcal{T}_A R_B + \mathcal{T}_B R_A} \times \frac{4\pi k_B T}{eV} \text{csch}\left(\frac{k_B T \pi}{E_c}\right) \left| \sin\left(\frac{eV}{2E_c}\right) \right|. \quad (21)$$

The visibility is a product of a term containing the QPC scattering probabilities and a function depending on the energy scales $k_B T$, eV and E_c . The scattering probability term is maximum for identical QPC's, $\mathcal{T}_A = \mathcal{T}_B$. The energy scale dependence is shown in Fig. 3 where the visibility for identical point contacts is plotted as a function of the normalized temperature, $k_B T/E_c$. We note several interesting features from Fig. 3 and Eq. (21). (i) the visibility shows decaying oscillations as a function of voltage $\nu_{I,MZ} \propto |\sin(eV/2E_c)|/eV$ for arbitrary temperature. (ii) A symmetric MZ-interferometer, $E_c \gg k_B T$,

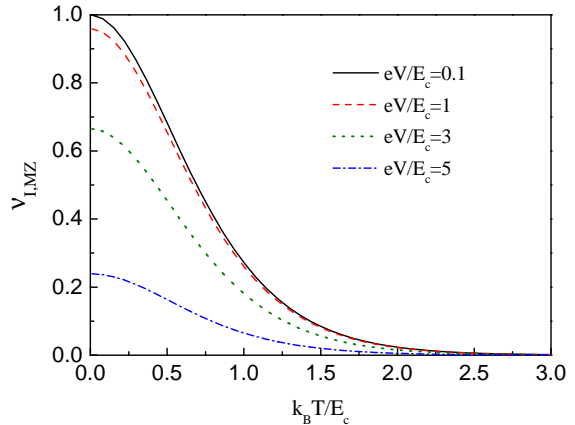


FIG. 3: Current visibility of the Mach-Zehnder interferometer $\nu_{I,MZ}$ versus normalized temperature $k_B T/E_c$ for $\mathcal{T}_A = \mathcal{T}_B$.

eV , has unity visibility (for $\mathcal{T}_A = \mathcal{T}_B$), i.e. shows perfect interference. (iii) The visibility decays monotonically with increasing temperature. For large temperatures, $k_B T \gg E_c$, the visibility decays exponentially with the temperature as $\nu_{I,MZ} \propto k_B T \exp(-\pi k_B T/E_c)$.

It is interesting to compare the calculated visibility to the experimentally measured one in Ref. [9]. As already shown in Ref [9], the measured scattering probability dependence of $\nu_{I,MZ}$ is well reproduced by Eq. (21). For the energy scale dependence, no information about the drift velocity v_D or the asymmetry ΔL needed to determine E_c is provided in Ref. [9]. However, to obtain the order of magnitude of E_c , considering as a rough estimate a typical drift velocity⁶³ $v_D \sim 10^4$ m/s at a magnetic field $B \sim 1T$ and an asymmetry $\Delta L \sim 0.1\mu\text{m}$ gives an E_c corresponding to an applied bias $\sim 10\mu\text{V}$ or a temperature $\sim 100\text{mK}$. These values are typically of the same order of magnitude as the ones considered in the experiment. As a first approximation, one would thus expect asymmetry effects to be of importance. The observed temperature dependence, a strong decrease of the visibility for increased temperature, is also qualitatively described by Eq. (21) with an $E_c/k_B \sim 50$ mK. This is however not the case with the voltage dependence. Ji et al find a differential visibility, i.e. the visibility of $dI(V)/dV$, which decays strongly with applied voltage, while Eq. (19) predicts a constant, voltage independent differential visibility. There are several possible explanations to why the voltage dependence in contrast to the temperature dependence is not reproduced by the theory. Ji et al themselves point out two voltage dependent dephasing mechanism: low frequency noise of $1/f$ type due to moving impurities, induced by a higher current and fast fluctuations of the potential landscape (and hence of the phase via the enclosed area) caused by screening of the additional charges injected at higher current. Screening might also, for the nonlinear current-voltage characteristics predicted by Eq. (19), lead to a voltage

dependent renormalization of the transmission probabilities, introducing a voltage dependence in the differential visibility.^{50,64} We also note that in the model of Ref. [16], inducing dephasing by coupling the MZ-interferometer to a quantum bath, gives a dephasing rate that increases with increasing voltage. Clearly, further investigations are needed to clarify the origin of the dephasing in the experiment in Ref. [9].

Turning to the noise, we focus on the cross correlator between currents flowing in terminals 3 and 4 (the auto-correlator can be obtained analogously). This allows for a straightforward comparison to the result of the HBT-interferometer, for which the cross correlator was investigated in Ref. [27]. From Eqs. (8) and (9) and the expressions for the scattering amplitudes, we arrive at the noise spectral density

$$S_{34}(E) = \frac{-2e^2}{h} [f(E) - f_0(E)]^2 \times \left\{ c_0 + c_\Theta \cos\left(\frac{E}{E_c} + \Theta\right) + c_{2\Theta} \cos\left(2\left[\frac{E}{E_c} + \Theta\right]\right) \right\}, \quad (22)$$

with coefficients

$$\begin{aligned} c_0 &= \mathcal{T}_A R_A + \mathcal{T}_B R_B - 6\mathcal{T}_A R_A \mathcal{T}_B R_B, \\ c_\Theta &= 2(\mathcal{T}_A - R_A)(\mathcal{T}_B - R_B) \sqrt{\mathcal{T}_A \mathcal{T}_B R_A R_B}, \\ c_{2\Theta} &= 2\mathcal{T}_A \mathcal{T}_B R_A R_B. \end{aligned} \quad (23)$$

Performing the energy integrals in Eq. (8) we find for the cross correlator

$$S_{34} = -\frac{2e^2}{h} \left\{ c_0 \bar{S}_0 + c_\Theta \bar{S}_\Theta \cos\left(\frac{eV}{2E_c} + \Theta\right) + c_{2\Theta} \bar{S}_{2\Theta} \cos\left[2\left(\frac{eV}{2E_c} + \Theta\right)\right] \right\} \quad (24)$$

where we introduce the functions

$$\bar{S}_0 = eV \coth \frac{eV}{2k_B T} - 2k_B T, \quad (25)$$

$$\begin{aligned} \bar{S}_\Theta &= 2\pi k_B T \operatorname{csch}\left(\frac{\pi k_B T}{E_c}\right) \left[\coth\left(\frac{eV}{2k_B T}\right) \right. \\ &\quad \left. \times \sin\left(\frac{eV}{2E_c}\right) - \frac{k_B T}{E_c} \cos\left(\frac{eV}{2E_c}\right) \right]. \end{aligned} \quad (26)$$

and

$$\begin{aligned} \bar{S}_{2\Theta} &= 2\pi k_B T \operatorname{csch}\left(\frac{2\pi k_B T}{E_c}\right) \left[\coth\left(\frac{eV}{2k_B T}\right) \right. \\ &\quad \left. \times \sin\left(\frac{eV}{E_c}\right) - \frac{2k_B T}{E_c} \cos\left(\frac{eV}{E_c}\right) \right]. \end{aligned} \quad (27)$$

containing the dependence on the energy scales eV , $k_B T$ and E_c .

Just as the current in Eq. (19), the noise consists of a phase independent, incoherent part and a phase dependent, interference part. However, in contrast to the

current, the phase dependent part of the noise contains two terms with different periods in Θ , corresponding to oscillations periodic in h/e and $h/2e$. These terms result from two-particle scattering processes which enclose the AB-flux one and two times respectively. Similarly to the current, the phase of the oscillations are shifted for a bias eV of the order of the asymmetry energy E_c .

It is important to note that in the MZ (in contrast to the HBT) interferometer, two particle and higher order scattering processes are just products of single particle scattering processes. The full distribution of current fluctuations¹⁷ is thus a function of single particle scattering probabilities only. In particular, the noise spectral density $S_{34}(E)$ in Eq. (22) is proportional to $-|s_{41}|^2 |s_{31}|^2$, i.e. partition noise¹ with phase dependent scattering probabilities. As a consequence, the phase independent, incoherent part of the noise can not be understood as partition noise from incoherent single particle processes, i.e. $\langle |s_{41}|^2 \rangle_{inc} \langle |s_{31}|^2 \rangle_{inc} \neq \langle |s_{41}|^2 |s_{31}|^2 \rangle_{inc}$. This is formally clear since the term proportional to $\cos^2 \Theta = [1 + \cos(2\Theta)]/2$, from two coherent scattering processes, obviously contribute to the phase independent part of the noise. As a consequence, as shown by Marquardt and Bruder,^{14,15} a model² with a filled stream of classical particles injected from reservoir 1 correctly reproduces the incoherent part of the current but fails to reproduce the incoherent part of the noise. In contrast, as found in Ref. [15] and further discussed below, the completely dephasing voltage probe model correctly reproduces the incoherent part of both the current and the noise.

To quantify the strength of the oscillations we introduce two separate quantities, $\nu_{N,MZ}^\Theta$ and $\nu_{N,MZ}^{2\Theta}$, here simply called visibilities, which in close analogy to the current visibility in Eq. (21) are defined as the ratio of the amplitudes of the noise oscillations and the average noise. They become

$$\nu_{N,MZ}^\Theta = \frac{|c_\Theta \bar{S}_\Theta|}{c_0 \bar{S}_0} \quad (28)$$

and

$$\nu_{N,MZ}^{2\Theta} = \frac{|c_{2\Theta} \bar{S}_{2\Theta}|}{c_0 \bar{S}_0}. \quad (29)$$

Similarly to the current, both visibilities are products of a term containing the scattering probabilities and a function of the energy scales eV , $k_B T$ and E_c . We first focus on the scattering probability dependent term by considering the visibility in the limit of a symmetric interferometer, $E_c \gg eV$, $k_B T$, where the energy-scale dependent terms are unity. This gives

$$\nu_{N,MZ}^\Theta = \frac{2|(\mathcal{T}_A - R_A)(\mathcal{T}_B - R_B)| \sqrt{\mathcal{T}_A \mathcal{T}_B R_A R_B}}{\mathcal{T}_A R_A + \mathcal{T}_B R_B - 6\mathcal{T}_A R_A \mathcal{T}_B R_B} \quad (30)$$

and

$$\nu_{N,MZ}^{2\Theta} = \frac{2\mathcal{T}_A \mathcal{T}_B R_A R_B}{\mathcal{T}_A R_A + \mathcal{T}_B R_B - 6\mathcal{T}_A R_A \mathcal{T}_B R_B}. \quad (31)$$

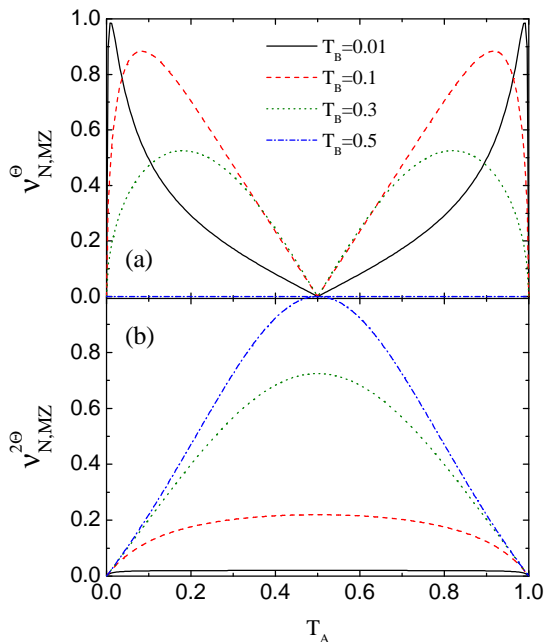


FIG. 4: Noise visibility $\nu_{N,MZ}^{\Theta}$ [figure (a)] of the h/e and $\nu_{N,MZ}^{2\Theta}$ [figure (b)] of the $h/2e$ oscillations in the shot noise of the Mach-Zehnder interferometer versus transmission \mathcal{T}_A of beam splitter A for $E_c \gg k_B T, eV$ for various transmission probabilities \mathcal{T}_B of beam splitter B .

The two visibilities are plotted in Fig. 4. Both visibilities are symmetric under the substitutions $\mathcal{T}_A \leftrightarrow R_A$ and $\mathcal{T}_B \leftrightarrow R_B$. The visibility $\nu_{N,MZ}^{\Theta}$ is zero for $\mathcal{T}_A = R_A = 1/2$, i.e. for a symmetric setting of any of the QPC's. The visibility increases for increasing QPC asymmetry, reaching a maximum for $0 < \mathcal{T}_A < 0.5$ and $0 < \mathcal{T}_B < 0.5$ (unity only in the limit $\mathcal{T}_A, \mathcal{T}_B \ll 1$) and then decreases again toward zero at $\mathcal{T}_A = 0$ or $\mathcal{T}_B = 0$. Interestingly, the visibility $\nu_{N,MZ}^{2\Theta}$ shows an opposite behavior. It is maximum, equal to unity, at $\mathcal{T}_A = \mathcal{T}_B = 1/2$ and then decreases monotonically for increasing QPC asymmetry, reaching zero at $\mathcal{T}_A = 0$ or $\mathcal{T}_B = 0$. This different dependence on the scattering probabilities makes it possible to investigate the two oscillations independently by modulating the QPC transparencies.

Turning to the energy scale behavior, we consider for simplicity $\nu_{N,MZ}^{\Theta}$ in the limit $\mathcal{T}_A, \mathcal{T}_B \ll 1$ and $\nu_{N,MZ}^{2\Theta}$ in the limit $\mathcal{T}_A = \mathcal{T}_B = 1/2$ where respective scattering probability terms are unity. For a symmetric interferometer, i. e. $E_c \gg eV, k_B T$, both visibilities are unity. Considering the situation when the temperature is comparable to the asymmetry energy scale E_c but the voltage is small $eV \ll k_B T, E_c$, we get the visibilities

$$\nu_{N,MZ}^{\Theta} = \frac{\pi k_B T}{E_c} \operatorname{csch} \left(\frac{\pi k_B T}{E_c} \right) \left[1 + \left(\frac{k_B T}{E_c} \right)^2 \right] \quad (32)$$

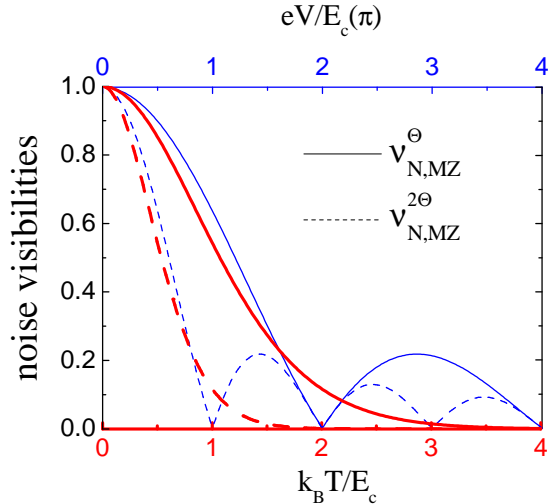


FIG. 5: Noise visibilities $\nu_{N,MZ}^{\Theta}$ (for $\mathcal{T}_A, \mathcal{T}_B \ll 1$) of the h/e and $\nu_{N,MZ}^{2\Theta}$ of the $h/2e$ oscillations in the shot noise correlation of a Mach-Zehnder interferometer for $\mathcal{T}_A = \mathcal{T}_B = 1/2$ versus $k_B T/E_c$ for $eV \ll k_B T, E_c$ (red curve) and versus eV/E_c for $k_B T \ll E_c, eV$ (blue curve).

and

$$\nu_{N,MZ}^{2\Theta} = \frac{2\pi k_B T}{E_c} \operatorname{csch} \left(\frac{2\pi k_B T}{E_c} \right) \left[1 + 4 \left(\frac{k_B T}{E_c} \right)^2 \right]. \quad (33)$$

The temperature dependence of the visibilities are shown in Fig. 5. Both visibilities decrease monotonically with increasing temperature. For large temperature $k_B T \gg E_c$, the visibilities decay exponentially as $\nu_{N,MZ}^{\Theta} \propto (k_B T)^3 \exp(-\pi k_B T/E_c)$ and $\nu_{N,MZ}^{2\Theta} \propto (k_B T)^3 \exp(-2\pi k_B T/E_c)$. The visibility $\nu_{N,MZ}^{\Theta}$ is thus considerably more sensitivity to thermal smearing than $\nu_{N,MZ}^{2\Theta}$. In the opposite limit, for a small temperature but a voltage comparable to E_c , i.e. $k_B T \ll E_c, eV$, we instead get the visibilities

$$\nu_{N,MZ}^{\Theta} = \frac{2E_c}{eV} \left| \sin \left(\frac{eV}{2E_c} \right) \right| \quad (34)$$

and

$$\nu_{N,MZ}^{2\Theta} = \frac{E_c}{eV} \left| \sin \left(\frac{eV}{E_c} \right) \right| \quad (35)$$

The visibilities as a function of voltage are plotted in Fig. 5. Both visibilities show an oscillating behavior, decaying as a power law $\propto 1/eV$ with increasing voltage. The period of oscillations, in eV , is $2\pi E_c$ for $\nu_{N,MZ}^{\Theta}$ but πE_c for $\nu_{N,MZ}^{2\Theta}$, half the value for $\nu_{N,MZ}^{\Theta}$. The different voltage dependence gives an additional possibility to investigate the two visibilities independently.

In the experiment of Ji et al.⁹ the noise was measured in the high voltage regime, with the interference terms in both the current and noise completely suppressed. The dependence of the incoherent noise on the transparencies \mathcal{T}_A and \mathcal{T}_B was investigated (\mathcal{T}_A was kept at 1/2 and \mathcal{T}_B was varied). A good agreement was found with the first, incoherent term in Eq. (24). Taken the open questions on the effect of decoherence on the average current, a detailed experimental investigation on the phase dependent, interference part of the noise would be of great interest.

A. Effect of dephasing

Next we consider the effect of dephasing on the current and noise. As discussed above, dephasing is introduced by connecting one of the two arms of the interferometer to a fictitious, dephasing voltage probe. The interferometer with the probe, denoted terminal 5, is shown in Fig. 6. The dephasing probe is connected to the edge via a contact described by a scattering matrix

$$\begin{pmatrix} \sqrt{1-\varepsilon} & i\sqrt{\varepsilon} \\ i\sqrt{\varepsilon} & \sqrt{1-\varepsilon} \end{pmatrix}, \quad (36)$$

where the dephasing parameter ε varies between 0 (no dephasing, fully coherent transport) and 1 (complete dephasing, fully incoherent transport). The presence of the dephasing probe modifies the amplitudes for scattering between the terminal 1, 2, 3 and 4. As an example, the scattering amplitude s_{41} , given in Eq. (16) in the absence of dephasing, now becomes

$$s_{41}(\varepsilon) = i\sqrt{\mathcal{T}_B R_A} e^{i(\phi_1 + \psi_1)} + i\sqrt{1-\varepsilon} \sqrt{\mathcal{T}_A R_B} e^{i(\phi_2 - \psi_2)}. \quad (37)$$

In addition, amplitudes for scattering into and out from the probe terminal 5 have to be considered. The current is obtained from Eqs. (4), (5) and (12). For the current in terminal 4, we find

$$I_4^{dp} = \frac{e}{h} [(\mathcal{T}_A R_B + \mathcal{T}_B R_A) eV + \sqrt{1-\varepsilon} \sqrt{\mathcal{T}_A \mathcal{T}_B R_A R_B} 4\pi k_B T \text{csch}\left(\frac{k_B T \pi}{E_c}\right) \times \sin\left(\frac{eV}{2E_c}\right) \cos\left(\frac{eV}{2E_c} + \Theta\right)]. \quad (38)$$

Comparison with the result in the absence of dephasing in Eq. (19) shows that the effect of the dephasing is to suppress the phase-dependent oscillations by multiplying the phase-dependent interference term with a factor $\sqrt{1-\varepsilon}$. For complete dephasing $\varepsilon = 1$, the phase dependent term is completely suppressed. The effect of dephasing can thus be simply incorporated in the visibility as

$$\nu_{I,MZ}^{dp} = \sqrt{1-\varepsilon} \nu_{I,MZ}, \quad (39)$$

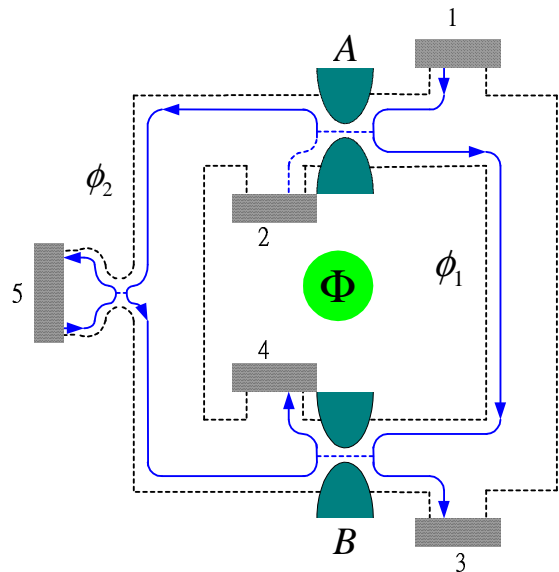


FIG. 6: The electrical MZ-interferometer, Fig. 2, with a dephasing voltage probe, 5, attached along one edge.

where $\nu_{I,MZ}$ is the visibility of the current oscillations in the absence of dephasing, given by Eq. (21). As is clear from the discussion above, to account for the experimental observations in Ref. [9], one would have to consider a voltage dependent dephasing parameter ε .

Turning to the noise, we obtain the cross correlator between currents in lead 3 and 4 in the presence of dephasing from Eqs. (8) and (14), giving

$$S_{34}^{dp} = -\frac{2e^2}{h} \left\{ c_0 \bar{S}_0 + c_\Theta \bar{S}_\Theta \sqrt{1-\varepsilon} \cos\left(\frac{eV}{2E_c} + \Theta\right) + c_{2\Theta} \bar{S}_{2\Theta} (1-\varepsilon) \cos\left[2\left(\frac{eV}{2E_c} + \Theta\right)\right] \right\}. \quad (40)$$

Here the terms c_0 , c_Θ , $c_{2\Theta}$, \bar{S}_0 , \bar{S}_Θ and $\bar{S}_{2\Theta}$ are defined above in Eqs. (23) and (25) and (27). Similarly to the current, the effect of the dephasing is only to suppress the amplitude of the phase-dependent oscillations. That is what one would naively expect to be the consequence of pure dephasing. The two phase-dependent terms are however affected differently, the $\cos \Theta$ term is suppressed by a factor $\sqrt{1-\varepsilon}$ while the $\cos 2\Theta$ term is suppressed by $(1-\varepsilon)$. The $\cos 2\Theta$ oscillations are thus more strongly suppressed. The visibilities of the two oscillations in the presence of dephasing can simply be written

$$\nu_{N,MZ}^{\Theta,dp} = \sqrt{1-\varepsilon} \nu_{N,MZ}^\Theta \quad (41)$$

and

$$\nu_{N,MZ}^{2\Theta,dp} = (1-\varepsilon) \nu_{N,MZ}^{2\Theta}, \quad (42)$$

where $\nu_{N,MZ}^\Theta$ and $\nu_{N,MZ}^{2\Theta}$ are the visibilities for the noise oscillations in the absence of dephasing, given by Eqs. (28) and (29), respectively.

Importantly, both oscillating terms are fully suppressed for complete dephasing, $\varepsilon = 1$. Complete dephasing within the voltage probe model thus gives a noise expression that only consists of the phase independent, incoherent term in Eq. (22). We note already here that the same result is found below for the HBT-interferometer. Since quantum interference by definition is excluded from the model, i.e. all scattering phases are neglected, the completely dephasing voltage probe thus constitutes a classical model that correctly reproduces the incoherent part of the noise. As pointed out above, a more detailed discussion of the physics of the voltage probe and a comparison with Refs. [14,15,59] is deferred to a later work.

It is interesting to note that the effect of dephasing introduced with the voltage probe, both for the current and noise, is for arbitrary dephasing strength identical to a phase averaging. The result in Eqs. (41) and (42) can be obtained by averaging the fully coherent expressions in Eqs. (28) and (29) with respect to a Lorentzian distribution $\rho(\Theta)$ of slow fluctuations of the phase Θ around the average value Θ_0 , as

$$\int d\Theta \rho(\Theta) \cos(n\Theta) = (1 - \varepsilon)^{n/2} \cos(n\Theta_0). \quad (43)$$

with the Lorentzian distribution

$$\rho(\Theta) = \frac{a/\pi}{(\Theta - \Theta_0)^2 + a^2}, \quad a = -(1/2)\ln(1 - \varepsilon) \quad (44)$$

We note that, as pointed out in Ref. [15], a Gaussian distribution of the phase fluctuations gives a different result, not consistent with the dephasing voltage probe approach for arbitrary dephasing strength.

We emphasize that the results above are independent on to which edge the probe is connected. Moreover, we also point out that the effect of the voltage probes, for arbitrary ε , is multiplicative, i.e. attaching n voltage probes at arbitrary places along the arms can be described by renormalizing $1 - \varepsilon \rightarrow (1 - \varepsilon)^n$. Writing $(1 - \varepsilon)^n = \exp(n\ln[1 - \varepsilon]) = \exp(-L/L_\phi)$, with $L_\phi = -d/\ln[1 - \varepsilon]$ and $L = nd$ with d the distance between two probes, we can quite naturally incorporate the effect of a uniform distribution of probes into a dephasing length L_ϕ . The suppression of the visibilities of the h/e and $h/2e$ oscillations due to dephasing in Eqs. (41) and (42) are then modified as $(1 - \varepsilon)^{1/2} \rightarrow \exp(-L/2L_\phi)$ and $(1 - \varepsilon) \rightarrow \exp(-L/L_\phi)$.

IV. HANBURY BROWN TWISS INTERFEROMETERS

The HBT-interferometer is less well known than the MZ-interferometer and deserves some additional comments.⁶⁵ The HBT-interferometer was invented as a tool to measure the angular diameter of stars. The first measurement¹⁸ was carried out on a radio star in 1954. Compared to existing schemes based on Michelson interferometers, the HBT-interferometer proved to be less

sensitive to atmospheric scintillations, which allowed for a more accurate determination of the angular diameter. After having demonstrated a table-top version of the interferometer in the visual range,¹⁹ the angular diameter of the visual star Sirius was determined.²⁰

The experimental results, both the two-particle interference and the positive intensity cross correlations, were successfully explained within a semi-classical framework. Soon after the experiments, it was however shown by Purcell⁶⁶ that the positive cross correlations could be explained in terms of bunching of individual photons, emerging from the star, a thermal source of light. This bunching was also demonstrated explicitly in subsequent photo counting experiments.^{67,68} The HBT experiment thus laid the foundations for quantum statistical methods in quantum optics.⁶⁹ The HBT approach has also been of importance in experimental particle physics.⁷⁰ It is interesting to note that positive intensity cross correlations between beams of light emerging from a thermal source, according to some contemporary^{71,72} “*would call for a major revision of some fundamental concepts in quantum mechanics*”. Purcell,⁶⁶ however, providing an elegant explanation of the bunching phenomena, pointed out that “*the Hanbury Brown Twiss effect, far from requiring a revision of quantum mechanics, is an instructive illustration of its elementary principles*”.

An optical table-top version^{73,74} of the HBT-interferometer is shown in Fig. 7. A beam of light is emitted from each one of the sources 2 and 3, completely uncorrelated with each other. The beams are split in two partial beams at the semitransparent beam splitters C and D respectively. The partial beams acquire phases ϕ_1 to ϕ_4 before scattering at the second pair of beam splitters A and B . The resulting beams are collected in detectors at ports 5 to 8.

Importantly, there is no interference pattern in the intensities at the detectors 5 to 8, instead the interference occurs only in the cross correlations between intensities at 5,6 and 7,8. The intensity cross correlations are sensitive to the two-particle amplitudes: the interference is thus between two different two-particle scattering events, e.g. (i) one particle from 2 scatters to 5 and one particle from 3 scatters to 8, with an amplitude $A_1 \exp(i[\phi_1 + \phi_2])$ and (ii) one particle from 2 scatters to 8 and one particle from 3 scatters to 5, with an amplitude $A_2 \exp(i[\phi_3 + \phi_4])$. The amplitude to detect one particle in 5 and one in 8 is then the sum of the two two-particle amplitudes. This is the case since both scattering processes have the same initial and final states and can not be distinguished. The (reducible) cross correlation between intensities in 5 and 8 is directly related to the corresponding two-particle probability $|A_1 \exp(i[\phi_1 + \phi_2]) + A_2 \exp(i[\phi_3 + \phi_4])|^2 = |A_1|^2 + |A_2|^2 + 2\text{Re}\{A_1 A_2^* \exp(i[\phi_1 + \phi_2 - \phi_3 - \phi_4])\}$. The interference term $2\text{Re}\{A_1 A_2^* \exp(i[\phi_1 + \phi_2 - \phi_3 - \phi_4])\}$ contains the four geometrical phases ϕ_1 to ϕ_4 . The HBT-interferometer is thus, in contrast to the MZ-interferometer, a two-particle interferometer.

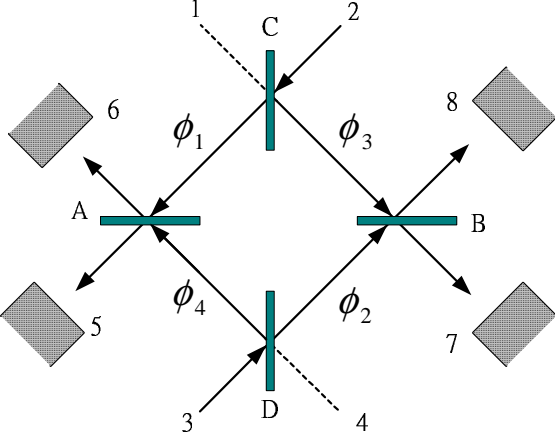


FIG. 7: Two-source, four-detector optical Hanbury Brown Twiss geometry proposed in Ref. [27]. Two beams of light incident from 2 and 3 are split in partial beams at the semi-transparent beam splitters C and D . The partial beams acquire geometrical phases ϕ_1 to ϕ_4 and are rejoined in the beam splitters A and B . The light intensity is measured in detectors 5 to 8

The electrical analog of the HBT-interferometer, presented in Ref. [27], is shown in Fig. 8. It consists of a (rectangular) conductor with a hole in the middle, a Corbino geometry. Similar to the MZ-interferometer, the electrons propagate along single edge states. Scattering between the edge states take place only at the beam splitters A to D . The beam splitters are described by scattering matrices given by Eq. (15). We first consider the fully coherent case. In contrast to the MZ-interferometer, the scattering amplitudes contain the phases ϕ_i and ψ_i only via multiplicative phase factors. As an example, the amplitude to scatter from terminal 2 to terminal 5 is given by

$$s_{52} = \sqrt{\mathcal{T}_A \mathcal{T}_C} e^{i(\phi_1 - \psi_1)}. \quad (45)$$

As a consequence, the average currents which depend only on the modulus squared of the scattering amplitudes [see Eqs. (4) and (6)] do not contain any scattering phases. We get the currents at terminals 5 to 8 as

$$\begin{aligned} I_5 &= (e^2/h)V (\mathcal{T}_A \mathcal{T}_C + R_A R_D), \\ I_6 &= (e^2/h)V (\mathcal{T}_A R_D + R_A \mathcal{T}_C), \\ I_7 &= (e^2/h)V (\mathcal{T}_B R_C + R_B \mathcal{T}_D), \\ I_8 &= (e^2/h)V (\mathcal{T}_B \mathcal{T}_D + R_B R_C). \end{aligned} \quad (46)$$

Turning to the current noise, the correlation between currents in terminals 5,6 and 7,8 is given by Eq. (9). We find for the spectral density for the correlators between terminal 5 and 8

$$\begin{aligned} S_{58}(E) &= \frac{-2e^2}{h} [f(E) - f_0(E)]^2 \\ &\times \{c_{0,58} + c_\Theta \cos(E/E_c + \Theta)\} \end{aligned} \quad (47)$$

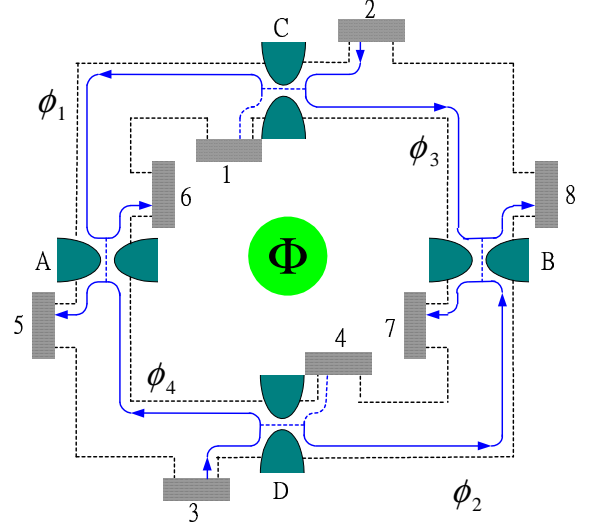


FIG. 8: Two-source, four-detector electrical Hanbury Brown Twiss geometry implemented in a conductor in the Quantum Hall regime. The electronic reservoirs 2 and 3 biased at eV and reservoirs 1 and 4 to 8 are kept at ground. The edge states (solid lines) have a direction of transport indicated by arrows. The QPC's A and B play the role of the beam splitters in Fig. 7. Geometrical phases ϕ_1 to ϕ_4 and the AB-flux Φ are shown.

with the coefficients

$$\begin{aligned} c_{0,58} &= \mathcal{T}_A R_B \mathcal{T}_C R_C + \mathcal{T}_B R_A \mathcal{T}_D R_D; \\ \bar{c}_\Theta &= 2 \prod_{j=A,B,C,D} \sqrt{\mathcal{T}_j R_j}, \end{aligned} \quad (48)$$

and for the correlator between terminal 5 and 7

$$\begin{aligned} S_{57}(E) &= \frac{-2e^2}{h} [f(E) - f_0(E)]^2 \\ &\times \{c_{0,57} + \bar{c}_\Theta \cos(E/E_c + \Theta)\} \end{aligned} \quad (49)$$

with the coefficient

$$c_{0,57} = \mathcal{T}_A \mathcal{T}_B \mathcal{T}_C R_C + R_A R_B \mathcal{T}_D R_D. \quad (50)$$

Performing the energy integrals in Eq. (9), we obtain the corresponding current cross correlators

$$S_{58} = \frac{-2e^2}{h} \left[c_{0,58} \bar{S}_0 + \bar{c}_\Theta \bar{S}_\Theta \cos\left(\frac{eV}{2E_c} + \Theta\right) \right] \quad (51)$$

and

$$S_{57} = \frac{-2e^2}{h} \left[c_{0,57} \bar{S}_0 + \bar{c}_\Theta \bar{S}_\Theta \cos\left(\frac{eV}{2E_c} + \Theta\right) \right]. \quad (52)$$

Here \bar{S}_0 and \bar{S}_Θ are given by Eqs. (25) and (26). The other two correlators S_{67} and S_{68} are given by the substitutions $S_{67} = S_{58} (\mathcal{T}_C \leftrightarrow \mathcal{T}_D)$ and $S_{68} = S_{57} (\mathcal{T}_C \leftrightarrow \mathcal{T}_D)$. Here, as for the MZ-interferometer we have $\Theta = \Delta\phi(E_F) + 2\pi\Phi/\Phi_0$ with $\Delta\phi = \phi_1 + \phi_2 - \phi_3 - \phi_4$ and $\sum_{i=1}^4 \psi_i = 2\pi\Phi/\Phi_0$.

Several observations can be made from the results above, put in comparison with the result for the noise correlations for the MZ-interferometer in Eq. (24). Just as for the MZ-interferometer, the noise consists of an incoherent, phase independent part, and a coherent, interference part. The phase dependent part of the noise in Eqs. (51) and (52) however contains only one term. The amplitude of the oscillating term is a product of a scattering probability term and an energy-scale dependent function, just as for the MZ-interferometer. This phase dependent term has the same dependence on the phase Θ , the same voltage dependent phase shift as well as the same energy-scale dependence as the second term in Eq. (24). This is the case since they both arise from processes which enclose the AB-flux once. Despite the fact that in the HBT interferometer the AB-effect results from two-particle processes, the periodicity is determined by the single electron flux quantum h/e . The dependence on the scattering probabilities is however different, a consequence of the MZ and HBT interferometer geometries being different. Importantly, there is no term in the noise in Eqs. (51) and (52) that corresponds to the last term in Eq. (24), describing processes which enclose the AB-flux twice. We note that the elementary scattering processes in the HBT-interferometer, in contrast to the MZ-interferometer, are two-particle processes. An important consequence of this is that the incoherent, phase independent noise term in Eqs. (51) and (52) can directly be reproduced by a model with filled streams of classical particles incident from reservoirs 2 and 3.

Since there is only one phase-dependent term, the visibility of the phase-dependent oscillations can again be directly defined, giving for $\alpha = 5, 6$ and $\beta = 7, 8$

$$\nu_{N,HBT}^{\Theta,\alpha\beta} = \frac{|\bar{c}_\Theta \bar{S}_\Theta|}{c_{0,\alpha\beta} \bar{S}_0}. \quad (53)$$

Since the energy-scale dependence of the visibilities is identical to $\nu_{N,MZ}^\Theta$ for the MZ-interferometer in Eq. (28), shown in Fig. 5, we focus here only on the scattering probability terms. We thus consider the limit of a symmetric interferometer, $E_c \gg k_B T, eV$ for which the energy-scale dependent part is unity. Several symmetries exist, e.g. all visibilities $\nu_{N,HBT}^{\Theta,\alpha\beta}$ are unchanged by the substitutions $R_C \leftrightarrow T_C$ and $R_D \leftrightarrow T_D$. The visibility $\nu_{N,HBT}^{\Theta,58}$ is unity for scattering probabilities obeying $T_A R_B R_C T_C = T_B R_A R_D T_D$ and similar relations hold for the other visibilities. All visibilities go to zero for any of the transmission probabilities approaching either zero or unity. Focusing on the case with $T_C = T_D$ (or equivalently $T_C = R_D$), the visibilities are given by

$$\nu_{N,HBT}^{\Theta,58} = \nu_{N,HBT}^{\Theta,67} = \frac{2\sqrt{\mathcal{T}_A R_A \mathcal{T}_B R_B}}{\mathcal{T}_A R_B + \mathcal{T}_B R_A} \quad (54)$$

and

$$\nu_{N,HBT}^{\Theta,57} = \nu_{N,HBT}^{\Theta,68} = \frac{2\sqrt{\mathcal{T}_A R_A \mathcal{T}_B R_B}}{\mathcal{T}_A \mathcal{T}_B + R_A R_B}. \quad (55)$$

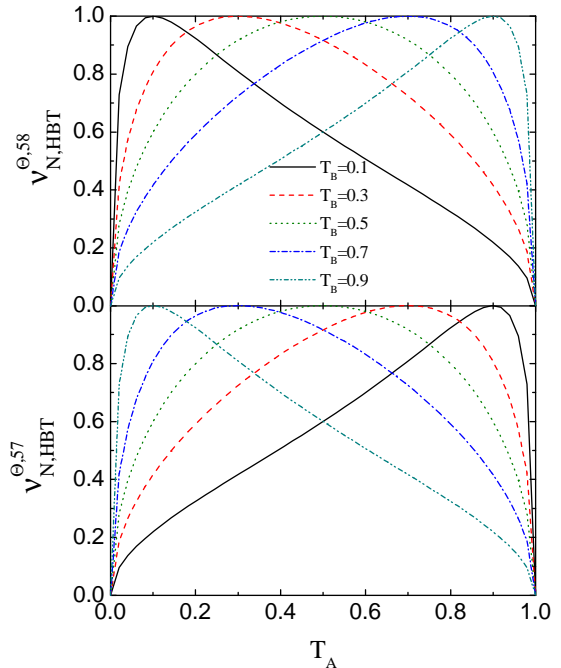


FIG. 9: Noise visibilities $\nu_{N,HBT}^{\Theta,58}$ and $\nu_{N,HBT}^{\Theta,57}$ of shot noise correlations in the HBT geometry versus transmission probability \mathcal{T}_A for various values of \mathcal{T}_B . A symmetric geometry, $E_c \gg kT, eV$, and identical QPC's C and D are considered.

The two different visibilities are plotted in Fig. 9 as a function of \mathcal{T}_A for different \mathcal{T}_B . The visibility $\nu_{N,HBT}^{\Theta,58}$ has a maximum equal to unity for $\mathcal{T}_A = \mathcal{T}_B$, while $\nu_{N,HBT}^{\Theta,57}$ instead has a maximum equal to unity for $\mathcal{T}_A = R_B$.

A. The effect of dephasing

Just as in the MZ-interferometer, the dephasing in the HBT-interferometer is introduced by connecting a fictitious voltage probe to an edge between any of the two point contacts. The HBT-interferometer with the probe, denoted 9, is shown in Fig. 10. Here the probe is connected to the edge between contact C and A, we emphasize that the results discussed below do not depend on to which edge-state the probe is connected.

The presence of the probe modifies the amplitudes for scattering from terminals 2, 3 to terminals 5 to 8. As an example, the scattering amplitude in Eq. (45) is modified

$$s_{52} = \sqrt{1 - \varepsilon} \sqrt{\mathcal{T}_A \mathcal{T}_C} e^{i(\phi_1 - \psi_1)}. \quad (56)$$

In addition, we also have to consider amplitudes for scattering into and out from the probe terminal 9. The average currents in the presence of dephasing, given from Eqs. (4) to (6) and (12), turn out to be given by the same

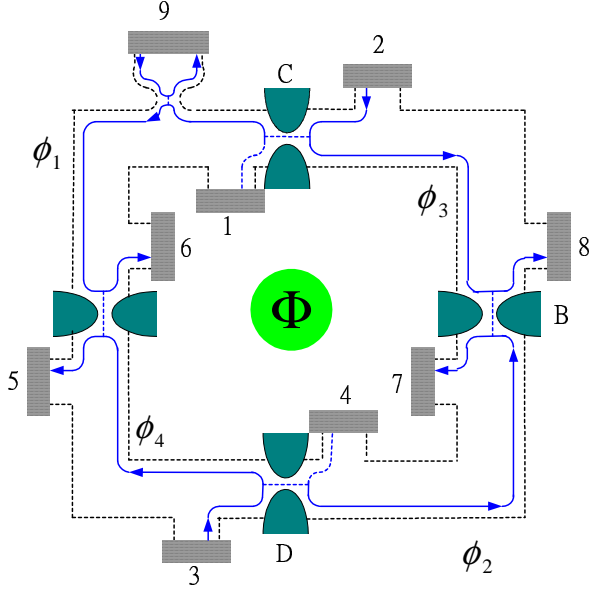


FIG. 10: The electrical HBT-interferometer, Fig. 8, with a dephasing voltage probe, 9, attached along one edge.

equations as in the absence of dephasing, i.e. Eq. (46). This is what one expects, i.e. that dephasing affects only the phase-dependent parts of the observables.

Turning to the current correlators, given from Eqs. (8), (9) and (14), we find for the correlators between terminal 5 and 8

$$S_{58}^{dp} = \frac{-2e^2}{h} \left[c_{0,58} \bar{S}_0 + \bar{c}_\Theta \bar{S}_\Theta \sqrt{1-\varepsilon} \cos \left(\frac{eV}{2E_c} + \Theta \right) \right] \quad (57)$$

and for the correlators between terminals 5 and 7

$$S_{57}^{dp} = \frac{-2e^2}{h} \left[c_{0,57} \bar{S}_0 + \bar{c}_\Theta \bar{S}_\Theta \sqrt{1-\varepsilon} \cos \left(\frac{eV}{2E_c} + \Theta \right) \right]. \quad (58)$$

The two remaining correlators are again given by the substitutions $S_{67} = S_{58} (\mathcal{T}_C \leftrightarrow \mathcal{T}_D)$ and $S_{68} = S_{57} (\mathcal{T}_C \leftrightarrow \mathcal{T}_D)$. We see from Eq. (57) and (58) that just as for the MZ-interferometer, the only effect of dephasing is to suppress the phase-dependent term. The suppression factor is $\sqrt{1-\varepsilon}$, just the same as for the $\cos \Theta$ term in the noise for the MZ-interferometer in Eq. (24). We can thus directly write the visibilities in the presence of dephasing as

$$\nu_{N,HBT}^{\Theta,\alpha\beta,dp} = \sqrt{1-\varepsilon} \nu_{N,HBT}^{\Theta,\alpha\beta}. \quad (59)$$

This leads to the conclusion that the voltage probe for the HBT-interferometer, just as for the MZ-interferometer, just has the same effect as dephasing due to slow fluctuations of the phase Θ , with the distribution of the phase fluctuations obeying the relation in Eq. (43). Moreover,

the voltage probes have the same multiplicative property as for the MZ-interferometer, allowing one to describe the effect of a continuum of probes along the edges (of total length $L = L_1 + L_2 + L_3 + L_4$) with a dephasing length L_ϕ . The suppression of the visibilities of the h/e oscillations due to dephasing are then modified as $(1-\varepsilon)^{1/2} \rightarrow \exp(-L/2L_\phi)$, just as for the h/e oscillations of the MZ-interferometer.

V. CONCLUSIONS

The MZ-interferometer is an amplitude interferometer: it exhibits a visibility in the average current with period h/e and exhibits a visibility in the shot noise with periods of both h/e and $h/2e$. In contrast, the HBT interferometer is an intensity interferometer, it exhibits no AB-effect in the current and exhibits only an h/e -effect in the shot noise correlations. Interestingly, our investigation shows that the shot noise visibility of the HBT interferometer as a function of temperature, voltage and dephasing rate, is qualitatively similar to that of the h/e -component of the shot noise of the MZ-interferometer. This is contrary to the naive expectation that the visibility of the two particle processes which lead to the HBT effect should be similar to the visibility of the two particle processes in the MZ-interferometer, that is the $h/2e$ component of the shot noise. Instead it is the number of times the AB-flux is enclosed which determines the behavior of the visibility.

In this paper we have investigated and compared in detail the voltage, temperature and asymmetry dependence for the current and noise visibilities in the MZ and HBT-interferometers. The experimental realization of the HBT-interferometer is of large importance since it allows for an unambiguous demonstration of two-particle interference effects with electrons, to date not demonstrated. Moreover, a successful realization of the HBT-interferometer would also enable a first demonstration of orbital entanglement in electrical conductors, a fundamentally important result. The results presented in this work should prove useful for the experimental work aiming to detect the HBT effect in electrical conductors.

VI. ACKNOWLEDGMENTS

We thank M. Heiblum, I. Neder, H. Förster and E. Sukhorukov for stimulating discussions. This work was supported by the Graduate Students Study Abroad Program, Taiwan National Science Council and the Taiwan NSC93-2112-M-009-036, the Swedish Research Council and the Swiss National Science Foundation and the network for Materials with Novel Electronic Properties.

-
- ¹ M. Büttiker, Phys. Rev. B **46**, 12485 (1992).
- ² Ya. Blanter and M. Büttiker, Phys. Rep. **336** 1(2000).
- ³ M. Born and E. Wolf, *Principles of Optics*, 7:th ed. (Cambridge University press, UK, 1999).
- ⁴ L. Mandel, Rev. Mod. Phys. **71**, S274 (1999).
- ⁵ See e.g. S. Pedersen, A.E. Hansen, A. Kristensen, C.B. Sorensen and P.E. Lindelof, Phys. Rev. B **61** 5457 (2000) and references therein.
- ⁶ E. Buks, R. Schuster, M. Heiblum, D. Mahalu and V. Umansky, Nature **391** 871 (1999).
- ⁷ A.E. Hansen, A. Kristensen, S. Pedersen, C.B. Sorensen, and P.E. Lindelof, Phys. Rev. B **64** 045327 (2001).
- ⁸ K. Kobayashi, H. Aikawa, S. Katsumoto and Y. Iye, J. Phys. Soc. Jpn., **71** 2094 (2002).
- ⁹ Y. Ji, Y. Chung, D. Sprinzak, M. Heiblum, D. Mahalu and H. Shtrikman, Nature **422**, 415 (2003).
- ¹⁰ G. Seelig, M. Büttiker, Phys. Rev. B **64**, 245313 (2001).
- ¹¹ G. Seelig, S. Pilgram, A.N. Jordan and M. Büttiker, Phys. Rev. B **68**, R161310 (2003).
- ¹² K. Le Hur, Phys. Rev. B **65**, 233314 (2002).
- ¹³ K. Le Hur, cond-mat/0503652.
- ¹⁴ F. Marquardt and C. Bruder, Phys. Rev. Lett. **92**, 56805 (2004).
- ¹⁵ F. Marquardt and C. Bruder, Phys. Rev. B **70**, 125305 (2004).
- ¹⁶ F. Marquardt, cond-mat/0410333.
- ¹⁷ H. Förster, S. Pilgram and M. Büttiker, cond-mat/0502400.
- ¹⁸ R. Hanbury Brown and R.Q. Twiss, Philos. Mag. Ser. 7 **45**, 663 (1954).
- ¹⁹ R. Hanbury Brown and R.Q. Twiss, Nature (London) **177**, 27 (1956).
- ²⁰ R. Hanbury Brown and R.Q. Twiss, Nature (London) **178**, 1046 (1956).
- ²¹ M. Henny, S. Oberholzer, C. Strunk, T. Heinzel, K. Ensslin, M. Holland and C. Schönenberger, Science **284**, 296 (1999).
- ²² W.D. Oliver, J. Kim, R.C. Liu, and Y. Yamamoto, Science **284**, 299 (1999).
- ²³ H. Kiesel, A. Renz, and F. Hasselbach, Nature (London) **418**, 392 (2002).
- ²⁴ M. Büttiker, Physica B **175**, 199 (1991).
- ²⁵ M. Büttiker, Phys. Rev. Lett. **68**, 843 (1992).
- ²⁶ D. Loss and E.V. Sukhorukov, Phys. Rev. Lett. **84**, 1035 (1992).
- ²⁷ P. Samuelsson, E.V. Sukhorukov, and M. Büttiker, Phys. Rev. Lett. **92**, 26805 (2004).
- ²⁸ K. v. Klitzing, G. Dorda, M. Pepper, Phys. Rev. Lett. **45**, 494 (1980).
- ²⁹ M. Büttiker, Phys. Rev. B **38**, 9375 (1988).
- ³⁰ B. I. Halperin, Phys. Rev. B **25**, 2185 (1982).
- ³¹ B. J. van Wees, H. van Houten, C. W. J. Beenakker, J. G. Williamson, L. P. Kouwenhoven, D. van der Marel, and C. T. Foxon, Phys. Rev. Lett. **60**, 848 (1988).
- ³² D. A. Wharam, T. J. Thornton, R. Newbury, M. Pepper, H. Ahmed, J. E. F. Frost, D. G. Hasko, D. C. Peacock, D. A. Ritchie and G. A. C. Jones, J. of Phys. C **21**, L861(1988).
- ³³ R.C. Liu, B. Odom, Y. Yamamoto, and S. Tarucha, Nature **391** 263 (1998).
- ³⁴ S. Oberholzer, M. Henny, C. Strunk, C. Schonenberger, T. Heinzel, K. Ensslin, M. Holland, Physica **6E**, 314 (2000).
- ³⁵ M. Büttiker, P. Samuelsson, E.V. Sukhorukov, Physica E **20**, 33 (2003).
- ³⁶ P. Samuelsson, E.V. Sukhorukov, and M. Büttiker, Phys. Rev. Lett. **91**, 157002 (2003).
- ³⁷ C.W.J. Beenakker, C. Emary, M. Kindermann, and J.L. van Velsen, Phys. Rev. Lett. **91**, 147901 (2003).
- ³⁸ C.W.J. Beenakker, and M. Kindermann, Phys. Rev. Lett. **92**, 056801 (2004).
- ³⁹ P. Samuelsson, and M. Büttiker, cond-mat/0410581 (Phys. Rev. B, in press).
- ⁴⁰ See also related work by C.W.J. Beenakker, M. Titov, B. Trauzettel, Phys. Rev. Lett. **94**, 186804 (2005); A. V. Lebedev, G. B. Lesovik, G. Blatter, cond-mat/0504583.
- ⁴¹ T. M. Stace, C. H. W. Barnes, and G. J. Milburn Phys. Rev. Lett. **93**, 126804 (2004).
- ⁴² L. Saminadayar, D. C. Glattli, Y. Jin and B. Etienne, Phys. Rev. Lett. **79**, 2526.2529 (1997).
- ⁴³ R. de-Picciotto, M. Reznikov, M. Heiblum, V. Umansky, G. Bunin, D. Mahalu, Nature **389** 162 (1997).
- ⁴⁴ I. Safi, P. Devillard, and T. Martin, Phys. Rev. Lett. **86**, 4628 (2001).
- ⁴⁵ S. Vishveshwara, Phys. Rev. Lett. **91**, 196803 (2003).
- ⁴⁶ S.A. Kivelson and V.L. Pokrovsky, Phys. Rev. B **40**, R1373 (1989).
- ⁴⁷ C. de C. Chamon, D.E. Freed, S.A. Kivelson, S.L. Sondhi and X.G. Wen, Phys. Rev. B **55**, 2331 (1997).
- ⁴⁸ M.R. Geller and D. Loss Phys. Rev. B **56**, 9692 (1997).
- ⁴⁹ T. Jonckheere, P. Devillard, A. Crepieux, Th. Martin, cond-mat/0503617.
- ⁵⁰ M. Büttiker, J. Phys. Condensed Matter **5**, 9361 (1993).
- ⁵¹ M. Büttiker, Phys. Rev. Lett. **57**, 1761 (1986).
- ⁵² M. Büttiker, Phys. Rev. Lett. **65**, 2901 (1990).
- ⁵³ M. Büttiker, Phys. Rev. B **33**, 3020 (1986).
- ⁵⁴ M. Büttiker, IBM J. Res. Dev. **32**, 63 (1988).
- ⁵⁵ C.W.J. Beenakker, and M. Büttiker, Phys. Rev. B **46**, 1889 (1992).
- ⁵⁶ M. J. M. de Jong, and C. W. J. Beenakker, Physica A **230**, 219 (1996).
- ⁵⁷ S. A. van Langen, and M. Büttiker, Phys. Rev. B **56**, R1680 (1997).
- ⁵⁸ C. Texier and M. Büttiker, Phys. Rev. B **62**, 7454 (2000).
- ⁵⁹ A.A. Clerk and A.D. Stone, Phys. Rev. B **69**, 245303 (2004).
- ⁶⁰ C.W.J. Beenakker and B. Michaelis, cond-mat/0503347.
- ⁶¹ D. B. Chklovskii, B. I. Shklovskii and L. I. Glazman, Phys. Rev. B **46**, 4026 (1992); N. R. Cooper and J. T. Chalker, Phys. Rev. B **48**, 4530 (1993).
- ⁶² H. A. Fertig, Phys. Rev. B **38**, 996 (1988).
- ⁶³ See e.g. the discussion in N. C. van der Vaart, M. P. de Ruyter van Steveninck, L. P. Kouwenhoven, A. T. Johnson, Y. V. Nazarov, C. J. P. M. Harmans, and C. T. Foxon, Phys. Rev. Lett. **73**, 320 (1994) and references therein.
- ⁶⁴ D. Sanchez and M. Büttiker, Phys. Rev. Lett. **93**, 106802 (2004); T. Christen and M. Büttiker, Phys. Rev. B **53** 2064, (1996).
- ⁶⁵ For an interesting historical account, see R. Hanbury Brown, *The Intensity Interferometer* (London: Taylor and Francis) 1974.
- ⁶⁶ E.M. Purcell, Nature **178**, 1449 (1956).

- ⁶⁷ R.Q. Twiss, A.G. Little, and R. Hanbury Brown, *Nature (London)* **180**, 324 (1957).
- ⁶⁸ G.A. Rebka, and R.V. Pound, *Nature (London)* **180**, 1035 (1957).
- ⁶⁹ See e.g. R. Loudon, *Rep. Prog. Phys.*, **43**, 58 (1980).
- ⁷⁰ G. Baym, *Acta Phys. Pol. B* **29**, 1839 (1998).
- ⁷¹ E. Brannen and H.I.S. Ferguson, *Nature (London)* **178**, 481 (1956).
- ⁷² R. Hanbury Brown and R.Q. Twiss, *Nature (London)* **178**, 1447 (1956).
- ⁷³ B. Yurke and D. Stoler, *Phys. Rev. Lett.* **68**, 1251 (1992).
- ⁷⁴ B. Yurke and D. Stoler, *Phys. Rev. A* **46**, 2229 (1992).